Hybrid of Opposite-Contrast MR Angiography (HOP-MRA) Combining Time-of-Flight and Flow-Sensitive Black-Blood Contrasts

Tokunori Kimura,[1*] Masato Ikedo,[1] and Syuhei Takemoto[2]

For the purpose of visualizing low-flow as well as high-flow blood vessels without using contrast agents, we propose a new technique called a hybrid of opposite-contrast MR angiography (HOP-MRA). HOP-MRA is a combination of standard time-of-flight (TOF) using a full first-order velocity-compensation for white-blood (WB) and flow-sensitive black-blood (FSBB) techniques, which use motion-probing gradients to introduce intravoxel flow dephasing. A dual-echo three-dimensional gradient echo sequence was used to reduce both imaging time and misregistration. HOP-MRA images were obtained using a simple-weighted subtraction (SWS) or a frequency-weighted subtraction (FWS) applying different spatial filtering for WB and BB images. We then assessed the relationships among the contrast-to-noise ratios (CNR) of the blood-to-background signals for those three images. In both volunteer and clinical brain studies, low-flow vessels were well visualized and the background signal was well suppressed by HOP-MRA compared with standard TOF- or BB-MRA. The FWS was better than the SWS when whole-maximum intensity projection was performed on a larger volume including with different types of tissue. The proposed HOP-MRA was proven to visualize low-flow to high-flow vessels and, therefore, demonstrates excellent potential to become a clinically useful technique, especially for visualizing collateral vessels which is difficult with standard TOF-MRA. Magn Reson Med 62:450–458, 2009.

Key words: MR; angiography; time-of-flight; black-blood; flow-sensitive; hybrid

To date, various MR angiography (MRA) techniques have been proposed using noncontrast enhancement (CE) for visualizing blood vessels (1,2). MRA techniques are roughly classified as white-blood (WB) (1–8) or black-blood (BB) (9–18) techniques according to the contrast between vessels and the background tissue. The WB- and BB-MRA techniques, respectively, visualize blood vessels with higher and lower signal intensities than the background tissue. In the WB techniques, time-of-flight (TOF) (3), subtraction (4–7), and phase contrast (PC) (8) methods have been proposed. The TOF method is a typical example of a WB-MRA and is most widely applied clinically, especially in the brain, due to its simplicity and robustness. TOF-MRA uses the inflow effect so that an artery with a high-flow velocity close to the inflow part of an imaging slab is visualized at a higher signal intensity. It is, however, difficult to visualize turbulent parts of flow, and peripheral and collateral vessels are not easily visualized. One subtraction method uses the difference of flow velocity between two cardiac phases (first introduced as an MRA method) (4), and another subtraction method is based on the difference of flow signals between the presence and absence of flow-rephasing gradients (5–7). However, as they require two different stages of imaging sequences, the acquisition time was twice that of the TOF method and misregistration artifacts often became problematic. The PC method can quantify flow velocity but is only used for special purposes as it requires 4 to 6 times the acquisition time of TOF-MRA.

In contrast, the BB method can correctly visualize slow-flow vessels and blood vessel walls. It is also possible with the BB method to visualize turbulent parts of flow which are difficult to visualize with the TOF method. A fast-spin-echo (FSE) method was initially used in a sequence of the BB method (9,10); however, very slow or recirculating flow vessels were difficult to visualize without incorporating an inversion recovery preparation pulse (11,12). In addition, the BB technique has an additional problem associated with the processing of minimum intensity projection (mIP); for example, it is difficult to exclude no-signal regions such as air using mIP with the BB method. Accordingly, BB techniques are currently not very widely used. Visualizing blood vessels using the WB method can be relatively easy using, for example, maximum intensity projection (MIP) (19). Another BB-MRA technique has been proposed which also enhances susceptibility contrast (13,14) and is useful for visualizing small veins. It is, however, not suitable for visualizing arteries. We have proposed an alternative BB technique known as flow-sensitive black-blood (FSBB), to visualize small vessels using 3D GRE with a motion-probing gradient to introduce intravoxel dephasing (15–18). We found FSBB to be very effective for visualizing smaller vessels, even using amplitude images with a relatively shorter TE than in SWI, despite its difficulty separating arteries and veins.

The above-mentioned conventional MRA methods have advantages and disadvantages in both of the WB and BB techniques, and these techniques are suitably used according to their intended purposes. However, it has been difficult for both techniques to clearly visualize the various structures of blood vessels. The purpose of this study is to propose and assess a new non-CE MRA technique that allows visualization of slow-flow to high-flow vessels

[1]MRI Systems Development Department, Toshiba Medical Systems Corp., Otawara-Shi, Tochigi-Ken, Japan.

[2]MRI Technical Support Department, Toshiba Medical Systems Corp., Otawara-Shi, Tochigi-Ken, Japan.

*Correspondence to: Tokunori Kimura, Toshiba Medical Systems Corporation, Systems Group, MRI Systems Development Department, MRI Systems Division, 1385, Shimoishigami, Otawara-Shi, Tochigi-Ken, 324-8550, Japan. E-mail: kimura@mr.nasu.toshiba.co.jp

Received 11 July 2008; revised 13 February 2009; accepted 18 February 2009.

DOI 10.1002/mrm.22021

Published online 12 June 2009 in Wiley InterScience (www.interscience.wiley.com).

when the imaging time is comparable to that for TOF-MRA.

THEORY

The basic idea for visualizing a wider flow range of vessels is to combine the TOF techniques that are excellent for high-flow vessels and the BB techniques that are excellent for low-flow vessels and then to synthesize these two data sets so as to enhance the blood-to-background contrast to noise ratio (CNR) without increasing the acquisition time or the misregistration. Figure 1 shows the schematic of the principle for obtaining HOP-MRA. When HOP-MRA is obtained by simple-weighted subtraction (SWS) of the WB signal (S_W) and the BB signal (S_B) using scaling factor α as:

$$S_H = S_W - \alpha S_B \quad [1]$$

as explained in the Appendix, that is that the ratio of blood-to-background CNR in HOP-MRA with SWS(CNR_H) to the blood-to-background CNR of WB (CNR_W) is generally given as a function of the contrast of WB (C_W), the contrast of BB (C_B), and α as:

$$CNR_H/CNR_W = (1 - \alpha C_B/C_W)/\sqrt{1 + \alpha^2} \quad [2]$$

The maximum CNR_H/CNR_W can be obtained when $\alpha = -C_B/C_W$, as:

$$[CNR_H/CNR_W]_{max} = \sqrt{1 + (C_B/C_W)^2} \quad [3]$$

Figure 2 demonstrates the relationship between the CNR_H/CNR_W and the parameters in Equation [2] and that for the optimal condition of the Equation [3]. As long as optimal α can be selected, depending on both vessel contrasts, the condition of $CNR_H/CNR_W > 1$ is always preserved. However, this optimal condition depends on vessel size and position in a single subject. When TOF is applied as a WB-MRA and FSBB is applied as a BB-MRA on HOP-MRA, the condition of $C_W < C_B$ is assumed to be satisfied for smaller vessels; in addition, absolute C_W for larger vessels (where $C_B/C_W > -1$) is regarded as sufficiently high. Accordingly, the CNR_H is preserved at almost the optimum level when α is approximately 1.5. This discussion is, however, adapted for localized areas including vessels. We must also consider the issue that background signals are usually not homogeneous in a single subject depending on tissue parameters, especially when dual-echo GRE is used and when MIP processing is applied to visualize three-dimensional (3D) volume data.

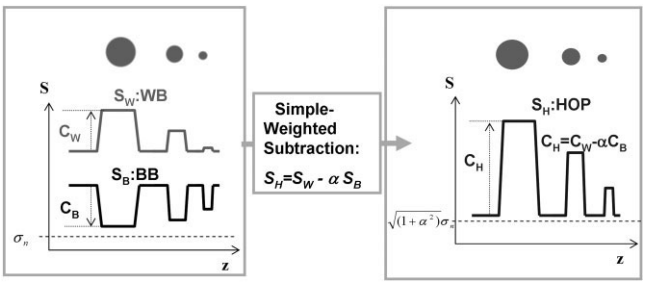

FIG. 1. Schematic of blood-vessel profiles for different sizes of different slab positions (z) in white blood: WB-, black-blood: BB-, and hybrid of opposite-contrast: HOP-MRA images. Blood-to-background contrasts for WB (TOF)- and BB (flow-sensitive black-blood: FSBB)-MRA, C_W, and C_B, become respectively positive and negative. Smaller vessels for FSBB have greater contrast than that for TOF, especially where far from the leading edge of the inflow direction and the signal intensities of the backgrounds for WB and BB are different because of the dual-echo acquisition. The vessel-to-background CNR for HOP-MRA obtained with a simple-weighted subtraction (SWS) between WB and BB, usually becomes greater despite noise enhancement to $\sqrt{(1 + \alpha^2)}$ times. See the Appendix regarding those definitions and derivations.

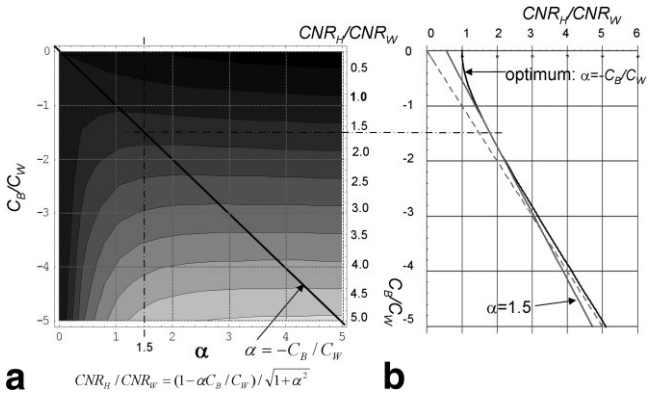

FIG. 2. **a:** Relative blood-to-background contrast noise ratio (CNR) mapping for HOP signal obtained with simple-weighted subtraction (SWS-HOP) shown as a ratio to the blood-to-background CNR of WB, (CNR_H/CNR_W), which is displayed in increments of 0.5 and is a function of two parameters of scaling α and the blood-to-background contrast ratio of BB to WB (C_B/C_W) given by Equation [2]. **b:** Maximum CNR_H/CNR_W as a function of C_B/C_W given by Equation [3] when $\alpha = -C_B/C_W$ in Equation [2] corresponding to the profile on the black line in Figure 2a and CNR_H/CNR_W at $\alpha = 1.5$. The optimal condition of CNR_H is almost preserved when α is approximately at 1.5 in this range as the condition of $C_B/C_W < -1$ can be assumed for smaller vessels in this technique. See Figure 1 and the Appendix regarding those definitions and derivations.

MATERIALS AND METHODS

Pulse Sequence

A dual-echo 3D gradient echo sequence was used to minimize both the acquisition time and the misregistration (Fig. 3). MTC pulses were not used on HOP-MRA to maintain the blood-to-background CNR for BB. In the first echo for TOF, TE1 = 6.4 ms (out-of-phase between water and fat at 1.5 Tesla [T]) and first-order gradient moment nulling (GMN) was applied on all three axes to reduce the displacement of the phase encoding artifacts of fast-flow vessels (20). In the second echo for FSBB, one should minimize TE2 to reduce the differences of signal intensity between two echoes caused by the T2* difference among different tissues, consider the chemical shift (fat-water) difference, and also apply flow dephasing gradients of suitable b-value to enhance low-flow vessels. Phase rewinder and spoiling gradients were applied after the second echo acquisition, and RF spoiling was also applied.

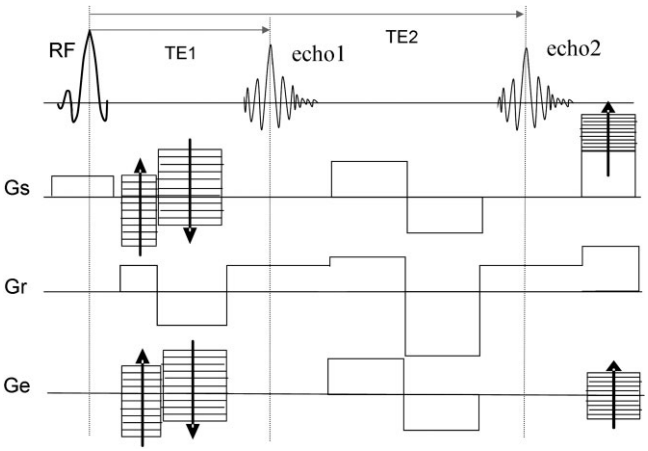

FIG. 3. Schematic for HOP-MRA sequence designed by 3D dual-gradient echo. The first echo is for WB (TOF), and the second echo is for BB (FSBB). First-order gradient moment nulling (GMN) was applied to all axes in the first echo to minimize the displacement of vessels. Motion-probing gradients were applied to the second echo to spoil the flowing spins in the blood vessels.

There is a trade-off relationship between the TE and the b-value. In this study, the first TE was fixed to the same TE as in the routine TOF, and the second TE was selected after optimizing the b-value by assessing the blood signal in FSBB.

Image Processing

One of two kinds of image processing was applied to the original data before MIP; the first was a SWS as shown in Equation [1]; the second was a frequency-weighted subtraction (FWS). In the FWS, different spatial filter operators, H_W for WB and H_B for BB, were applied and then subtracted to reduce the effects of the background signals and to enhance smaller vessels as:

$$S_H = H_W[S_W] - H_B[S_B] \quad [4]$$

When TOF is applied as a WB and FSBB is applied as a BB on HOP-MRA, the blood vessels in the BB data have relatively higher frequency components than those in the WB data and the susceptibility artifacts in the BB data have relatively lower frequency components, therefore, a different filter shape was designed for both the WB and the BB data. Figure 4 shows the typical shapes of the 1D positive quadrant of the 3D ellipsoidal-symmetric linear space invariant (LSI) filter applied to the FWS method shown as a function of normalized frequency k_n given as: $k_n^2 = (k_x/Kc_x)^2+(k_y/Kc_y)^2+(k_z/Kc_z)^2$ where Kc_x, Kc_y, and Kc_z are the respective cut-off frequency in 3D k-space (k_x, k_y, k_z) given $|k_x| \leqq Kc_x$, $|k_y| \leqq Kc_y$ and $|k_z| \leqq Kc_z$ when the acquisition matrix is $2Kc_x$x$2Kc_y$x$2Kc_z$. In this case, three different strengths of high-frequency enhancement filters generated in combination with standard filter and the high-pass filter for the FWS in 3D k-space, were used in contrast to the standard filter for the SWS, which has a uniform gain within a certain range toward the frequency direction. The same zero-frequency gain of BB for FWS as SWS, corresponding to α, provides a mutually similar low-frequency contrast, for example, the FWS for the case in Figure 4 provides a similar contrast to the SWS of α = 0.5. In this study, filtering was performed on each magnitude image and was then followed by subtraction. The ratio of the blood-to-background CNR to that of the WB, that is, CNR_H/CNR_W, for FWS was derived in the Appendix together with the SWS relationship.

After obtaining a synthesized image for HOP-MRA on the original WB and BB images using the SWS or FWS processes, MIP (19) was performed with (partial-MIP) or without (whole-MIP) volume selection.

Experiments

Imaging was performed on a 1.5-T whole-body imager (EXCELART Vantage™, Toshiba Medical Systems). A five-channel brain coil and parallel imaging with a SENSE factor of 2 were used. Several techniques for generating HOP-MRA were compared with standard TOF and TOF with MTC (MTC-TOF) (23) which are currently in clinical use. Volunteer and clinical data were obtained according to the regulations of our institution's internal review board after we received written informed patient consent. Typical parameters for normal volunteer data (Figs. 6 and 7) were: repetition time (TR) = 33 ms, echo time (TE: TE1/TE2) = 6.4/23.8 ms, flip angle (FA) = 20°, field of view (FOV) = 19 cm, slab thickness = 7 cm, acquisition matrix size = 208 × 256 × 80 (voxel size = 0.91 × 0.75 × 0.90 mm^3), and a double size of a sinc interpolation on every axis was performed by zero-filling in k-space. The

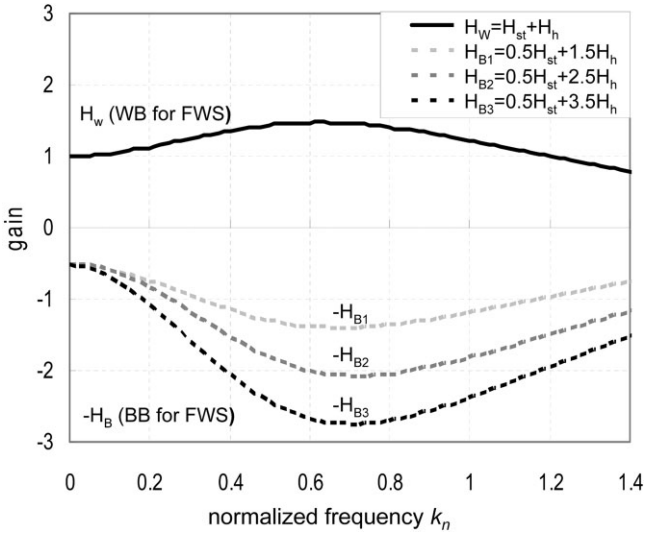

FIG. 4. Typical shapes of the 1D positive quadrant of the 3D ellipsoidal-symmetric linear space invariant (LSI) filters for WB (TOF) and BB (FSBB) in frequency-weighted subtraction (FWS) processing where the horizontal axis is a normalized frequency with the cut-off frequency, k_n (show text). As the filters for WB and BB are shown respectively with positive and negative gain, the difference at a certain frequency corresponds to the gain of the FWS-HOP signal. Three strengths of filters for BB obtained by weighted summation of the standard filter H_{st} and the high-pass filter H_h where the zero-frequency gain is 0.5, corresponding to half of the filter for WB, are shown.

same partial echo of 70% and a bandwidth of 122 Hz/pixel were used for both echoes to prevent subtraction error. The technique of inclined RF power toward a slab direction (ISCE) (22) of 1:2 (bottom:top) was commonly used. In the pulse sequence for MTC-TOF, a SORS type MTC pulse (23) of FA = 400° was added before every RF pulse. The two encoding gradients differed when first-order GMN was fulfilled only at zero frequency. Other parameters were the same as the TOF part of HOP-MRA. Imaging time was 5 min, 28 s for each method. Patient data were obtained with different parameters due to the gradient and central processing unit (CPU) performance, as follows: TR = 34 ms; TE1/TE2 = 6.4/27 ms; FA = 20°; FOV = 20 cm; slab thickness = 12 cm; acquisition matrix size = 256 × 256 × 80 (voxel size = 0.78 × 0.78 × 1.5 mm^3); and a double-size sinc interpolation was only performed on the slice axis. Other parameters were the same as those used with the volunteer data. Imaging time was 5 min, 43 s for each method. To assess the visibility of vessels depending on the vessel size and MRA methods, blood-to-background CNRs were measured on different vessels of different sizes, each vessel being measured with all three MRA methods.

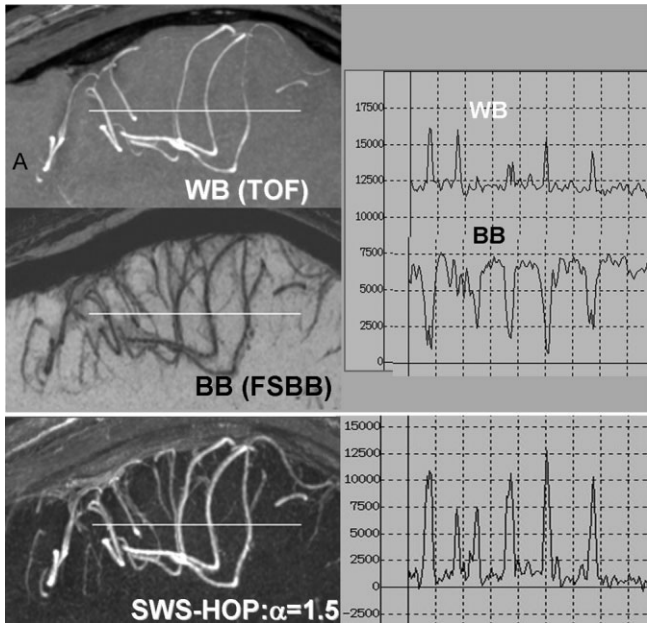

FIG. 5. MIPed (WB and SWS-HOP) and mIPed (BB) images and profiles from the first normal volunteer brain with thin slab thickness (2 cm) for WB-, BB-, and SWS-HOP-MRA with α = 1.5. Smaller vessels as well as larger vessels were well enhanced by positive contrast in SWS-HOP.

RESULTS

Figure 5 shows the MIPed or mIPed images and profiles obtained using TOF-, FSBB-, and SWS-HOP-MRA with α = 1.5 for the middle cerebral artery (MCA) region of a normal volunteer brain. Smaller vessels were well-visualized by HOP-MRA compared with standard TOF-MRA. Figure 6 shows MIPed or mIPed images obtained using different MRA techniques with the same receiver gain, including currently used MTC-TOF. In Figures 5 and 6, the axial MIP or miP were performed with a thinner slab-thickness (20 mm), excluding the skull base, to show the BB image. Figure 7 shows the blood-to-background CNR for each method in the same data set as Figure 6 where the background was selected for white matter and the noise level for different MRA methods was regarded as the same. The blood-to-background CNRs were obtained on the four portions of different vessel sizes of MCA, as shown by the dots on the original slice and the MIP image, including this slice for the SWS of α = 1.5. The CNRs for the largest vessels (MCA-L) of MTC-TOF were the best. Note that the smallest vessels (MCA-SS) resulted in the negative contrast in MTC-TOF and TOF but were enhanced by SWS- and FWS-HOP.

Regarding the SWS results in Figures 6 and 7, the blood-to-background CNR of smaller vessels for SWS-HOP-MRA increased with increasing α, as C_B/C_W was less than −1 as the blood vessels became smaller. This observation was consistent with the theoretical simulation of Figure 2. However, greater α (>1.5) introduced an increase in the background signals such as the muscle or fat signals in the scalp and negative signals (α = 2) smaller than the air portion in the brain parenchyma. A choice of α of approximately 1.5 is likely to be optimal if the MIP volume is within the brain parenchyma.

Regarding the results for FWS in Figures 6 and 7, the local CNRs for smaller vessels on the original slice were reduced for the FWS rather than for the SWS, due to the noise effects induced by a high-frequency enhancement filter for FWS, as shown in the Appendix. The exclusive feature for the FWS is, however, to allow smaller vessels to be enhanced while preserving the similar low-frequency contrasts of background tissue for a SWS of α = 0.5 as demonstrated in Figure 6.

When comparing the various MRA images obtained on whole-MIP of thicker slabs (Fig. 8), the smaller vessels on the vertical MIP image by SWS-HOP were better visualized than those by either MTC-TOF or standard TOF, and the effects of the background signals in the scalp were minor when axial MIP without volume selection was used. Although the vessels were visualized sufficiently by SWS-HOP when the MIP volume was within the brain parenchyma, as shown in Figure 6, the susceptibility effects on BB worsened the visibility of vessels, especially when the skull base was included in the MIP volume. In contrast, FWS-HOP dramatically improved the visualization of the vessels in any MIP direction even when the MIP volume included the base of the skull, despite SNR reduction in the intracranial tissue; furthermore, the effects of background signals on SWS-HOP were reduced by FWS-HOP. Venous signals visualized by SWS-HOP were reduced with FWS-HOP, especially in larger vessels such as the transverse sinus.

In the case of right MCA occlusion without symptoms (Fig. 9), SWS-HOP could better visualize the smaller vessels in the occluded hemisphere than TOF, although the scalp signal interfered with those signals even on axial MIP images due to the thicker slab of 12 cm (including the top of the head). In contrast, FWS-HOP could visualize collateral vessels in the area of the occluded MCA even on MIP without volume selection in any direction.

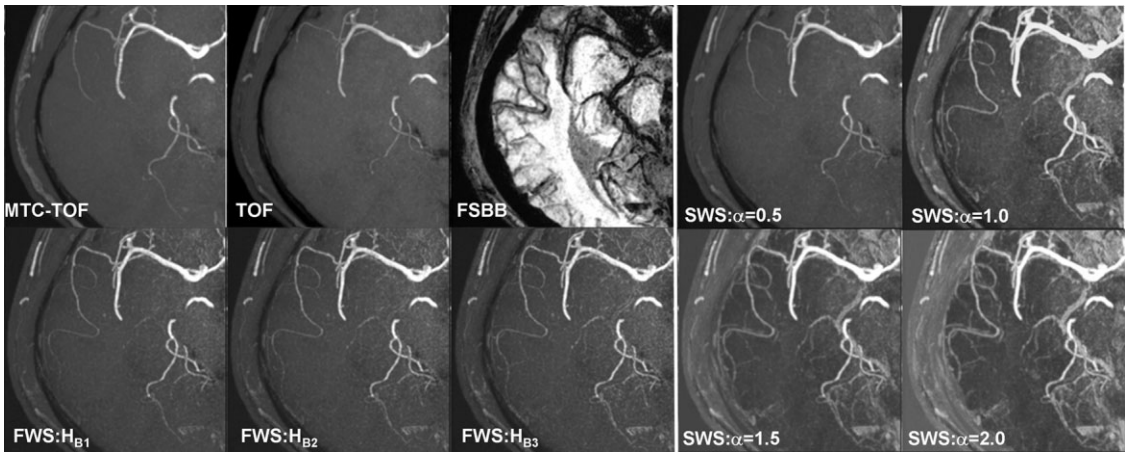

FIG. 6. MIPed or mIPed images obtained using five different types of MRA techniques from the second normal volunteer brain. Left top row shows the MTC-TOF, TOF, and FSBB images; left second row shows three different FWS-HOP images, and at right are four different SWS-HOP images. Here the slab thickness was 2 cm and the zero-frequency gain for the FWS was the same as that for the SWS of $\alpha = 0.5$.

DISCUSSION

We have demonstrated that HOP-MRA can contribute to enhancing the dynamic range of visualizing blood vessels by combining different pulse sequences of TOF and FSBB and simple image processing. Regarding the pulse sequence for HOP-MRA, using a shorter TE for FSBB while keeping a sufficient b-value is likely to further improve the visibility of vessels on HOP-MRA due to the reduction of dependency on the background signals induced by the T2* differences of different types of tissue. Regarding the dependency on chemical shift for fat/water, it was better to select an in-phase TE than the out-phase for the second echo because the background signals of the fat region on HOP-MRA was reduced by subtracting the higher signals of BB. The FSBB technique with suitable MPGs introducing intravoxel flow-dephasing, highly contributed to the visibility of smaller vessels on HOP-MRA, as shown in Figure 7. A b-value of approximately 2 (s/mm^2) was sufficient for successful visualization of smaller vessels when using our imaging parameters. Here, MPGs on all three axes were applied simultaneously to introduce higher dispersion effects while keeping a shorter TE. Thus, the direction of coherent flow may have an effect on the blood-to-background CNR, especially when quantitative measurements are made. The aliasing effects of the negative phase in vessels sometimes reduced the blood-to-back-

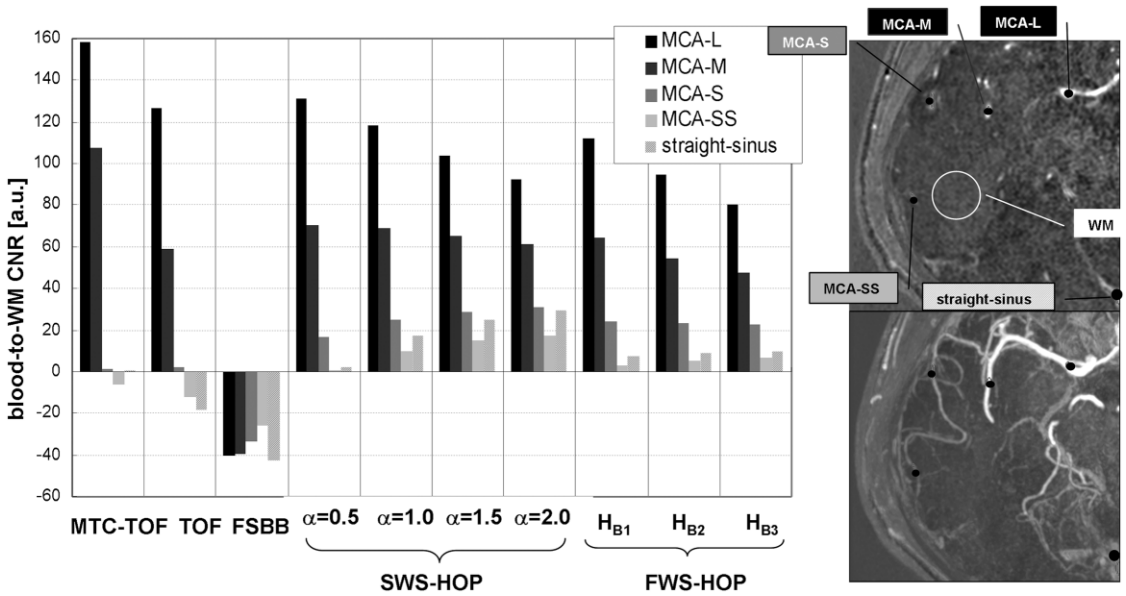

FIG. 7. Blood-to-white matter (WM) CNR measured in the same data set as Figure 6. Each was measured in four portions (L, M, S, and SS toward the peripheral) in the right middle cerebral artery (MCA) and in the straight sinus, as shown by the dots on the original slice of the slab center. Note that the smallest vessel, that is, MCA-SS, for the TOF shows negative contrast but is enhanced and shows positive contrast in the SWS and FWS-HOP images.

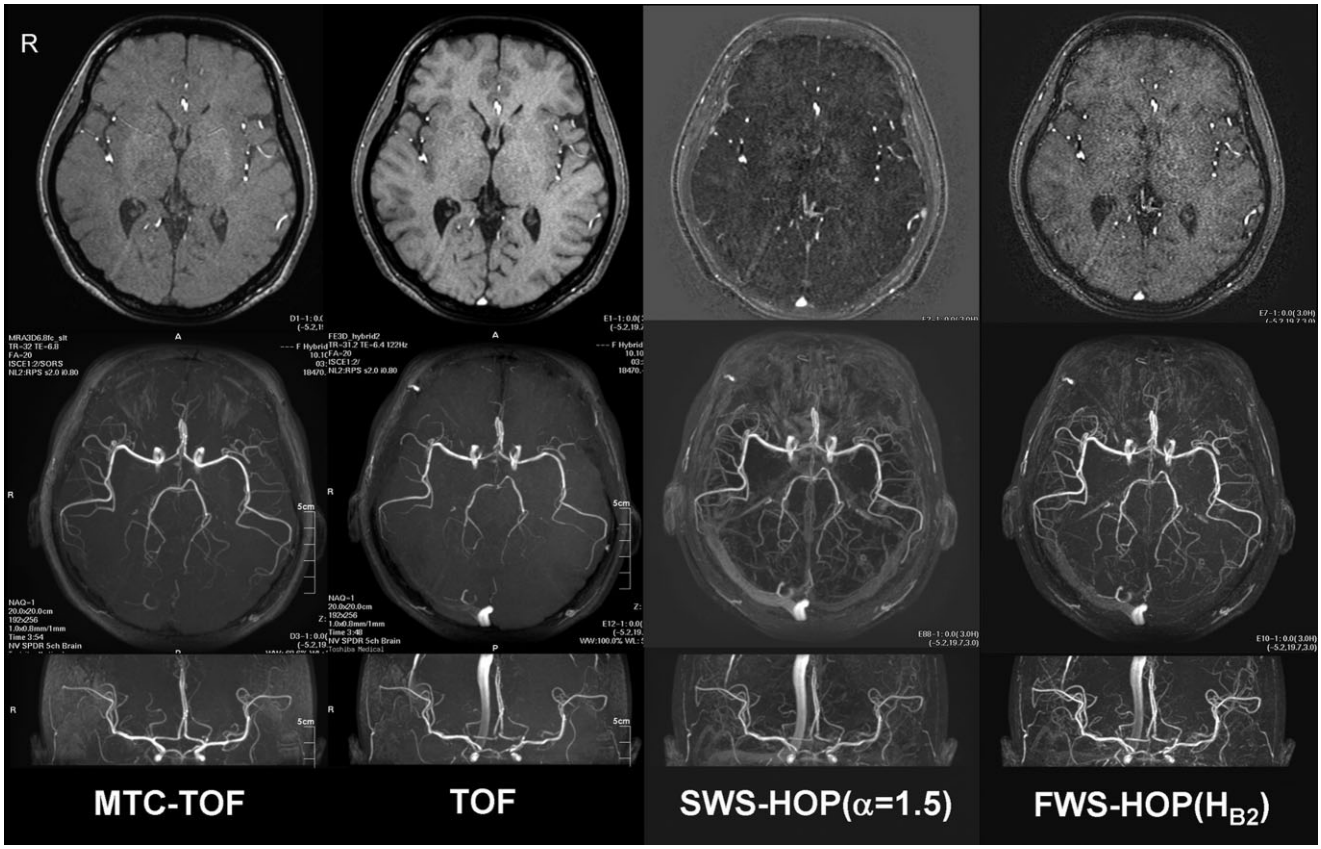

FIG. 8. Comparison of different MRA techniques for the third normal volunteer brain. The top row is the single-slice image (center of the slab), the second row is on axial-MIP, and the bottom row consists of frontal-MIP images, where whole-MIP was performed with a slab thickness = 7 cm (thicker than in Fig.5 and Fig. 6), and each imaging time was 3 min, 50 s. The smaller vessels on SWS-HOP were better visualized than those on MTC-TOF or on TOF, but were disturbed by background artifacts. In contrast, FWS-HOP improved the background artifacts as well as the vessel visualization even on MIP with a thicker slab.

ground CNR. It is, however, not likely to be a serious a problem in MRA used for obtaining anatomic information. Acquiring data with a single-slab rather than multiple slabs (24) is better for HOP-MRA in contrast to standard TOF, which is used to improve the CNR of slow-flow vessels due to the dominant contribution from FSBB data. Separate sequence approaches rather than this dual-echo sequence are also available for WB and BB to obtain HOP-MRA if motion between the two acquisitions is negligible or correctable while preserving CNR per unit time. It is considered that the flow-dephasing effects for the second data in the previous investigations (4,5) were not sufficient to allow visualization of small vessels compared with our technique. It should be easy in 2D acquisitions, just as in 3D acquisitions, to alternate WB and BB in an interleaved manner, e.g., per slice-encoding. A combination of different sequence types, such as steady-state free progression and GRE, might also be available and the difference in background signals is likely to be reduced using the FWS technique. Original sliced images of MTC-TOF generally cannot be used instead of T1W images as the MTC pulse introduces a reduction of CNR for tissues of different T1, as shown in Figure 8. However, HOP-MRA ensures sufficient MRA contrast for major arteries without adding an MTC pulse as the original blood-to-vessel CNR for such arteries is sufficiently high, as shown in Figure 6. Avoiding an MTC pulse in HOP-MRA is rather effective, not only to reduce the specific absorption rate (SAR) but also to enhance T1W contrast of TOF images.

Image processing was very important in HOP-MRA to visualize the required vessels while reducing the problems associated with the TE difference of WB and BB obtained by dual-echo GRE acquisition. Here, two kinds of methods called SWS and FWS were assessed. When there is tissue with greater signal than the blood vessel in the viewing direction while processing MIP, the vessels are invisible even though the localized blood-to-background CNR is greater. Tissues with shorter T1 and T2*, such as muscle or fat, or tissues near bone or air and with greater susceptibility effects, introduce higher signal in GRE-based SWS-HOP images when α is increased. When partial-MIP within homogeneous tissue, such as brain parenchyma, is performed, it is enough to apply SWS by selecting suitable α to visualize the vessels while suppressing background signals. The main feature of the FWS technique, compared with SWS, is to allow the vessels to be visualized even when using whole-MIP without volume selection due to the effects of reducing tissue-dependent background signals by decreasing the low-frequency gain for FSBB. This feature permits simple automatic processing after acquisi-

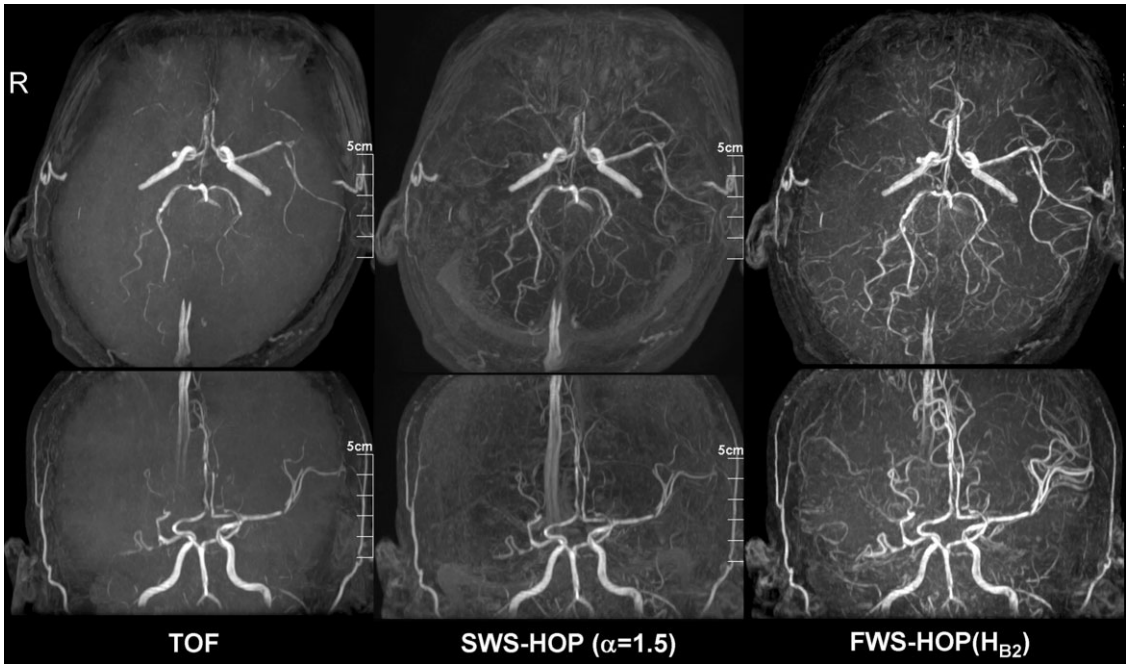

FIG. 9. Clinical MRA of a right MCA occlusion (arrow) compared using three techniques for each of the axial-MIP (top low) and frontal-MIP (bottom low) images. Collateral vessels in the MCA area were best visualized on the FWS-HOP image although they were visualized vaguely on TOF and even on SWS-HOP. Here, whole-MIP with a slab thickness = 12 cm was performed.

tion. As FWS also contributes to reducing the susceptibility artifacts introduced by longer TE for FSBB. TE may have to be shortened for higher field MRI so as to reduce the susceptibility artifacts. The problem of SNR reduction in FWS is caused by the enhancement of the higher frequency portions by the LSI type filters used for simplicity in this implementation. This problem, however, will be solved by using an adaptive type of high pass filter. As Alexander et al. used a median filter to reduce the background signal effects in FSE-based (25) or GRE-based BB images (26), that is likely to be an alternative filter for FWS-HOP. The problems of viewing vessels with SWS-HOP are also likely to be solved if an intelligent user interface is combined with SWS images, i.e., if MIP volume or scaling α can be selected interactively while checking the MIP images.

HOP-MRA was able to visualize smaller vessels well, however, major arteries, especially those under the position of the Circle of Willis, were only improved in visualization to a slight extent compared with MTC-TOF. This was due to the weak contribution from those vessels in FSBB; that is, negative smaller C_B/C_W was introduced by tissue such as bone or air surrounding those vessels. In addition, gradient shapes for GMN in first echo (TOF) were likely to affect the visibility of turbulent portions, especially those in the bends of vessels. Further optimization of GMN is required in combination with first TE, considering the fat-water phase and to minimize phase-encoding displacement artifacts (20).

More recently, Du and Jin proposed a dual-echo technique for simultaneous acquisition of TOF-MRA and venography (27). Their technique uses first-order GMN for both echoes and then provides separate images; in contrast, our technique uses MPG for the second echo and then combines two echoes. Our technique also allows TOF and BB data to be acquired with a relatively short TR and to use the data separately, although our BB data includes arteries as well as veins.

Our proposed HOP-MRA technique allows the operator to simultaneously obtain T1W and T2*W 3D images as well as 3D-MRA with the same positions and with almost the same imaging time as MTC-TOF. This feature will contribute to better total patient throughput and to a reduction of the operator's workload.

CONCLUSION

We have presented a new technique called a hybrid of opposite-contrast MR angiography (HOP-MRA) technique and which is a combination of standard time-of-flight (TOF) and flow-sensitive black-blood (FSBB) methods. We demonstrated that it can improve visualization of small vessels compared with the standard TOF and also to MTC-TOF MRA and without increasing the imaging time. Although further technical optimization and clinical evaluation will be required, we believe that this technique will provide additional clinical information regarding slow-flow vessels, such as collaterals, which are difficult to visualize on conventional TOF-MRA. It also will provide user-friendly viewing compared with standard BB-MRA and thus demonstrates excellent potential to become an alternative technique to TOF-MRA.

ACKNOWLEDGMENTS

We thank K. Tsuchiya, MD, and K. Kobayashi, RT, from Kyorin University for providing clinical data and valuable

comments. We also thank W. Dannels, A. Wheaton, and M. Miyazaki, in our division, for providing technical advice and B. Hami, MA (USA) and R. Ahlberg (Japan English Service, Inc.) for editing this manuscript.

APPENDIX

CNR of HOP-MRA

Here, we consider the CNR of blood vessels when combining white-blood (WB) and black-blood (BB) images into HOP-MRA.

First, blood-to-background CNR in a simple-weighted subtraction (SWS) HOP image obtained by $S_H = S_W\text{-}\alpha S_B$, is derived when C_W and C_B are the respective contrasts between two types of original blood signals (S_W and S_B) and background tissue signals (S_{Wback} and S_{Bback}). From the definition of the problem, $C_W = S_W\text{-}S_{Wback}$, $C_B = S_B\text{-}S_{Bback}$, the blood-to-background contrast of the S_H image, $C_H = S_H\text{-}S_{Hback}$, can be expressed using only the contrasts of the original images as:

$$C_H = (S_W - \alpha S_B) - (S_{Wback} - \alpha S_{Bback}) = (S_W - S_{Wback}) - \alpha(S_B - S_{Bback}) = C_W - \alpha C_B \quad [A1]$$

A noise SD of SWS-HOP image, σ_{nH} is given using noise SDs of WB and BB image (σ_{nW} and σ_{nB}) as:

$$\sigma_{nH} = \sqrt{\sigma_{nW}^2 + \alpha^2\sigma_{nB}^2} \quad [A2]$$

The blood-to-background CNR of SWS-HOP image, CNR_H is thus given by:

$$CNR_H = C_H/\sigma_{nH} = (C_W - \alpha C_B)/\sqrt{\sigma_{nW}^2 + \alpha^2\sigma_{nB}^2} \quad [A3]$$

Here, the CNR of the S_H image is maximized under the following condition:

$$\partial(CNR_H)/\partial\alpha = (-\alpha C_W\sigma_{nB}^2 - C_B\sigma_{nW}^2)/(\sigma_{nW}^2 + \alpha^2\sigma_{nB}^2)^{3/2} = 0 \quad [A4]$$

When the denominator in Equation [A5] is not zero, the optimal α satisfying Equation [A6], is given by:

$$\alpha_{opt} = -(C_B/\sigma_{nB}^2)/(C_W/\sigma_{nW}^2) \quad [A5]$$

especially assuming that $\sigma_{nW} = \sigma_{nB} = \sigma_n$, Equation [A3] and Equation [A7] can be written as:

$$CNR_H = (C_W - \alpha C_B)/\{\sqrt{(1 + \alpha^2)}\sigma_n\} \quad [A6]$$

$$\alpha_{opt} = -C_B/C_W \quad [A7]$$

Equation [A6] can also be rewritten by using the ratio to the blood-to-background CNR of WB, $CNR_W = C_W/\sigma_n$, as:

$$CNR_H/CNR_W = (1 - \alpha C_B/C_W)/\{\sqrt{(1 + \alpha^2)}\} \quad [A8]$$

In summary, the CNR concerning the contrast between the blood vessel and the peripheral tissue in the weighted difference image of the two kinds of original images, is maximized when α is equal to a value that has inverted the sign of the ratio of the CNRs concerning the contrast between the blood vessel and the peripheral tissue in each of the two kinds of original images. When the subject is imaged with the same coil and with the same receiver gain and when the SWS method is applied, the above Equation [A6] and Equation [A7] were satisfied.

In contrast, when the frequency-weighted subtraction (FWS) method with LSI filters of $H_{W.fil}(k)$ and $H_{B.fil}(k)$ is applied, the blood-to-background contrasts for WB and BB are modified respective to $C_{W.fil}$ and $C_{B.fil}$, and the ratios of noise SD to the standard filter for SWS of $H_{st}(k)$ respectively become:

$$\sigma_{nW\cdot fil}/\sigma_{nW} = \int H_{W\cdot fil}(k)\,dk/\int H_{st}(k)\,dk,$$

and

$$\sigma_{nB\cdot fil}/\sigma_{nB} = \int H_{B\cdot fil}(k)\,dk/\int H_{st}(k)\,dk \quad [A9]$$

where the shapes of the filters are assumed to be circular (2D) or spherically (3D) symmetrical and the aliasing effects are ignored. Then, CNR_H for FWS processing (subtraction using filtered data: $S_H = S_{W.fil}\text{-}S_{B.fil}$) becomes:

$$CNR_H = (C_{W\cdot fil} - C_{B\cdot fil})/\left\{\sqrt{\{\sigma_{nW\cdot fil}^2 + \sigma_{nB\cdot fil}^2}\right.$$

$$= (C_{W\cdot fil} - C_{B\cdot fil})/\left[\sqrt{\begin{array}{c}\{\sigma_{nW}\cdot\int H_{W\cdot fil}(k)\,dk/\int H_{st}(k)\,dk\}^2 \\ +\{\sigma_{nW}\cdot\int H_{B\cdot fil}(k)\,dk/\int H_{st}(k)\,dk\}^2\end{array}}\right] \quad [A10]$$

especially, when $\sigma_{nW} = \sigma_{nB} = \sigma_n$, Equation [A10] will become:

$$CNR_H = (C_{W\cdot fil} - C_{B\cdot fil})/\left[\sigma_n\sqrt{\begin{array}{c}\{\int H_{W\cdot fil}(k)\,dk/\int H_{st}(k)\,dk\}^2 \\ +\{\int H_{B\cdot fil}(k)\,dk/\int H_{st}(k)\,dk\}^2\end{array}}\right] \quad [A11]$$

Note that, in Equation [A10] or Equation [A11], although the noise term in the denominator is enhanced, the contrast term of the numerator is further enhanced, especially in smaller vessels compared with the SWS method when there is the same zero-frequency gain combination between WB and BB.

REFERENCES

1. Ståhlberg F, Ericsson A, Nordell B, Thomsen C, Henriksen O, Person B. MR imaging, flow and motion. Acta Radiol 1992;33:179–200.
2. Miyazaki M, Lee VS. Nonenhanced MR angiography. Radiology 2008; 248:20–43.
3. Dumoulin CL, Hart HR Jr. Magnetic resonance angiography. Radiology 1986;161:717–720.
4. Wedeen VJ, Meuli RA, Edelman RR, Geller SC, Frank LR, Brady TJ, Rosen BR. Projective imaging of pulsatile flow with magnetic resonance. Science 1985;22:946–948.
5. Axel L, Morton D. MR flow imaging by velocity-compensated/uncompensated difference images. J Comput Assist Tomogr 1987;11:31–34.

6. Laub GA, Kaise WA. MR angiography with gradient motion refocusing. J Comput Assist Tomogr 1988;12:377–382.
7. Machida Y, Shinichi K, Nobuyasu I, Makita J, Hatanaka M, Goro T. Dual echo time 3D subtraction MR angiography of the head. Jpn Soc Med Imaging Tech 1992;10:414–422.
8. Moran PR. A flow velocity zeugmatographic interlace for NMR imaging in humans. Magn Reson Imaging 1982;1:197–203.
9. Edelman RR, Mattle HP, Wallner B, Bajakian R, Kleefield J, Kent C, Skillman JJ, Mendel JB, Atkinson DJ. Extracranial carotid arteries: evaluation with "black blood" MR angiography. Radiology 1990;177:45–50.
10. Alexander AL, Buswell HR, Sun Y, Chapman BE, Tsuruda JS, Parker DL. Intracranial black-blood MR angiography with high-resolution 3D fast spin echo. Magn Reson Med 1998;40:298–310.
11. Mayo JR, Culham JA, MacKay AL, Aikins DG. Blood MR signal suppression by preexcitation with inverting pulses. Radiology 1989;173: 269–271.
12. Parker DL, Goodrich KC, Masiker M, Tsuruda JS, Katzman GL. Improved efficiency in double-inversion fast spin-echo imaging. Magn Reson Med 2002;47:1017–1021.
13. Reichenbach JR, Barth M, Haacke EM, Klarhofer M, Kaiser WA, Moser E. High-resolution MR venography at 3.0 Tesla. J Comput Assist Tomogr 2000;24:949–957.
14. Haacke EM, Xu Y, Cheng YC, Reichenbach JR. Susceptibility weighted imaging (SWI). Magn Reson Med 2004;52:612–618.
15. Kimura T, Ikedo M, Furudate N, Takemoto S. Flow-sensitive susceptibility-weighted imaging. In: Proceedings of the 16th Annual Meeting of ISMRM, Berlin, Germany, 2007. (abstract 3015).
16. Tsuchiya K, Kimura T, Kobayashi K, Takemoto S. Flow-sensitive susceptibility-weighted imaging of the brain: initial experience in ischemic lesions. In: Proceedings of the 16th Annual Meeting of ISMRM, Berlin, Germany, 2007. (abstract 3016).
17. Kodama T, Yano T, Tamura S, Machida Y, Kimura T. Flow-sensitive black blood imaging for evaluating vascular malformations. In: Proceedings of the 17th Annual Meeting of ISMRM, Toronto, Canada, 2008. (abstract 3425).
18. Gotoh K, Okada T, Miki Y, Ikedo M, Ninomiya A, Kamae T, Togashi K. Visualization of the lenticulostriate artery with flow-sensitive black-blood imaging in comparison with time-of-flight MR angiography. In: Proceedings of the 17th Annual Meeting of ISMRM, Toronto, Canada, 2008. (abstract 2893).
19. Laub G. Displays for MR angiography. Magn Reson Med 1990;14:222–229.
20. Nishimura DG, Jackson JI, Pauly JM. On the nature and reduction of the displacement artifact in flow images. Magn Reson Med 1991;22:481–492.
21. Edelman RR, Ahn SS, Chien D, Li W, Goldmann A, Mantello M, Kramer J, Kleefield J. Improved time-of-flight MR angiography of the brain with magnetization transfer contrast. Radiology 1992;184:395–399.
22. Atkinson D, Brant-Zawadzki M, Gillan G, Purdy D, Laub G. Improved MR angiography: magnetization transfer suppression with variable flip angle excitation and increased resolution. Radiology 1994;190:890–894.
23. Miyazaki M, Kojima F, Ichinose N, Onozato Y, Igarashi H. A novel saturation transfer contrast method for 3D time-of-flight magnetic resonance angiography: a slice-selective off-resonance sinc pulse (SORS) technique. Magn Reson Med 1994;32:52–59.
24. Parker DL, Yuan C, Blatter DD. MR angiography by multiple thin slab 3D acquisition. Magn Reson Med 1991;17:434–451.
25. Alexander AL, Chapman BE, Tsuruda JS, Parker DL. A median filter for 3D FAST spin echo black blood images of cerebral vessels. Magn Reson Med 2000;43:310–313.
26. Kholmovski EG, Parker DL. High resolution magnetic resonance venography at 3 Tesla: optimized acquisition, reconstruction, and post-processing. In: Proceedings of the 14th Annual Meeting of ISMRM, Miami, Florida, USA, 2006. (abstract 810).
27. Du YP, Jin Z. Simultaneous acquisition of MR angiography and venography (MRAV). Magn Reson Med 2008;59:954–958.